

Improve the Interpretability of Attention: A Fast, Accurate, and Interpretable High-Resolution Attention Model

Tristan Gomez
Université de Nantes
tristan.gomez@etu.univ-nantes.fr

Suiyi Ling
Université de Nantes
suiyi.ling@univ-nantes.fr

Thomas Fréour
Université de Nantes, CHU Nantes,
Inserm, CRTI, Inserm UMR 1064,
F-44000 Nantes, France
thomas.freour@chu-nantes.fr

Harold Mouchère
Université de Nantes
harold.mouchere@univ-nantes.fr

February 28, 2024

Abstract

The prevalence of employing attention mechanisms has brought along concerns on the interpretability of attention distributions. Although it provides insights about how a model is operating, utilizing attention as the explanation of model predictions is still highly dubious. The community is still seeking more interpretable strategies for better identifying local active regions that contribute the most to the final decision. To improve the interpretability of existing attention models, we propose a novel Bilinear Representative Non-Parametric Attention (BR-NPA) strategy that captures the task-relevant human-interpretable information. The target model is first distilled to have higher-resolution intermediate feature maps. From which, representative features are then grouped based on local pairwise feature similarity, to produce finer-grained, more precise attention maps highlighting task-relevant parts of the input. The obtained attention maps are ranked according to the ‘active level’ of the compound feature, which provides information regarding the important level of the highlighted regions. The proposed model can be easily adapted in a wide variety of modern deep models, where classification is involved. It is also more accurate, faster, and with a smaller memory footprint than usual neural attention modules. Extensive experiments showcase more comprehensive visual explanations compared to the state-of-the-art visualization model across multiple tasks including few-shot classification, person re-identification, fine-grained image classification. The proposed visualization model sheds imperative light on how neural networks ‘pay their attention’ differently in different tasks.¹

1 Introduction

Thanks to the unprecedented booming of deep learning, many applications enjoyed a big leap in performance in the last decade. Nevertheless, these deep learning based methods are commonly considered as ‘black box’ approaches, where the internal functioning is unclear [27]. As one of the solutions to remedy this lack of interpretability, attention mechanism [3] are frequently employed for explaining the deep model. Yet to which extend those attention models help in interpreting how the model is operating has recently become a novel debate [4, 24]. An ideal interpretable attention model should not only be able to quantify the important level of a certain part of the neural network but also be capable of identifying precise local regions of the input to provide

¹Source codes are uploaded in supplemental materials and will be made available to the public after acceptance.

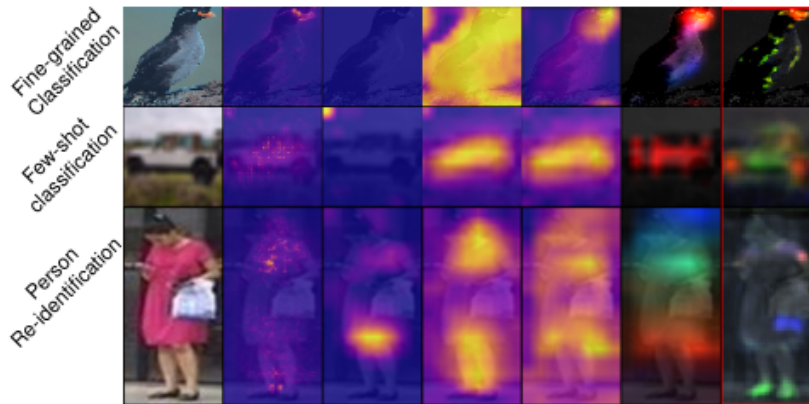


Figure 1: From left to right: original image, Guided Grad-CAM++, Grad-CAM, Grad-CAM++, activation map, B-CNN, BR-NPA. Our method yields precise attention maps focused on small details and highlights a potential hierarchy among the object’s parts relevance.

proper visual guidance regarding which key component is playing a greater role in the decision-making of the corresponding task [4]. To this end, in this study, we propose a novel framework that generates high-resolution interpretable attention maps without sacrificing the performance of the target model. More specifically, this framework improves the interpretability of the usual multi-part attention system designed for deep Convolutional Neural Network models (CNNs) in two ways: (1) we propose to increase the resolution of the output feature maps of a network and the attention map for finer details ; (2) we propose to replace the common learned attention layer [3] with a non-parametric layer that groups pixels based on their *active level*, and similarity with others. This layer does not require training, which constitutes a simpler function than the standard attention module made of convolutional layers. It produces comprehensive attention maps focusing on semantic parts of the input while being faster with a lower memory footprint.

Examples of multi-parts attention maps obtained using our method are shown in Fig. 1. Our algorithm is designed such that the importance level (in terms of contributions to the final decision-making of the task) of different salient parts of objects could be also friendly visualized via color. In Fig. 1, the 1st, 2nd, and 3rd most important attention maps are respectively represented in red, green, and blue. Inspection of the maps shows, for example, that the head of the bird is generally more important than its body in the task of fine-grained classification. Our method can be applied to various problems and produces attention maps adapted to the task at hand. On fine-grained classification and person re-identification, the model precisely highlights small details and discriminative parts whereas in few-shot classification, the model focus on the global object structure. Experiments on semantic segmentation show similar results to few-shot classification can also be found in supplemental materials.

In the spirit of calls for more interpretable attention model, the focal point of this contribution is to develop a more explainable and interpretable attention model that could be easily plugged into different applications. Although the proposed attention framework helps to boost the performances of some state-of-the-arts, we do not focus on making a contribution to improve the state-of-the-art in standard computer vision tasks, which is beyond the scope of this study.

2 Related works

Generic explanation methods: One of the most straightforward ways to identify which local component of the input contributes the most to the model decision-making is the Activation Map (AM) that simply outputs a heatmap showing the average activation across channels. However, not all the activated areas offer necessarily cues for accomplishing the target task, e.g., classifying a certain category. To overcome this drawback, more interpretable visualization approaches including the Class-Activation Map (CAM) [42], Grad-CAM [27] or

Grad-CAM++ [6] were proposed to locate the local task-relevant areas. In [29], the Guided-Backpropagation (GB) was proposed to visualize the gradients of the input image pixels and maximises the score of the predicted class, which generates high-resolution saliency maps. Based on these previous studies, it has also been proposed to combine Grad-CAM with GB to obtain a high-resolution map, *i.e.*, Guided Grad-CAM, that emphasizes the areas that are related to the prediction [27]. Guided Grad-CAM++ was proposed in [6] to further improve the interpretability of Grad-CAM.

Attention-based architecture for specific task: There are many existing attention-based models that were developed for fine-grained classification: Lin *et al.* proposed a bilinear CNN (B-CNN) that employs two distinct CNNs to obtain the feature maps from the intermediate convolutional layer just before the pooling layer, and further multiply them with outer product [20] to explore the coefficient between network features. Inspired by this work, in [16], it was proposed to generate the attention maps by integrating a convolutional module to the intermediate output feature. Several similar soft attention layer based models were also developed for the same purpose, including the multi-attention CNN (MA-CNN) [39] that uses a loss term to train an attention layer to group channels according to their similarity, and the Prototypical Part Network (ProtoPNet) [7] that matches learned feature vectors against the feature volume in the manner of a convolution. Several methods proposed to generate part-level crops using reinforcement learning like Fully Convolutional Attention Networks (FCAN) [22] or weakly-supervised learning like Spatial Transformer Networks (ST-CNN) [17], Multi-Granularity CNN (MG-CNN) [33] or MA-CNN [39]. There are also various neural attention layers that were designed for the task of person re-identification [38, 19, 8, 28]. The Relation-aware Global Attention (RGA) module was proposed in [38] to capture the global structural information. In [19], the authors suggest to jointly learn the soft and hard attentions along with simultaneous optimisation of feature representations. Some works have also been introduced to make full use of the particular modalities of the task of person re-identification by exploiting both spatial and temporal clues [8, 28]. There are also attention mechanisms that are tailored to few-shot/meta-learning algorithms. Several models were developed to better localize relevant object regions and improve sample efficiency [35, 15, 11]. Analogously, Zhu *et al.* propose to learn diverse and informative parts [43]. Recently, a unique module is presented to find relevant frames in a video [37]. Notwithstanding all the appalling attention existing task-specific attention models, one common trait of these works is that they yield attention methods that are tailored for only one typical task.

3 The Proposed Model

The proposed attention model is composed of (1) extracting high-resolution feature maps; (2) generating representative feature vectors obtained via grouping similar vectors together, and (3) concatenating the representative feature vectors and forwarding to the classification layer. In this study, the intermediate output of a convolutional network (layer), *i.e.*, a tensor with size of $C \times H \times W$, is defined as the *feature volume* or *feature maps*. Once a spatial position (h, w) is chosen, where $h \in [1, H], w \in [1, W]$, a vector of dimension C can be extracted, namely, the *feature vector*.

3.1 High-Resolution Feature Maps

Given a standard CNN, commonly, the size of the last feature map is significantly smaller than the one of the input. For example, after feeding an image of 448×448 to a ResNet-50 backbone [13] network, the size of the output feature map is reduced to 14×14 . This makes it difficult to interpret how the neural network was activated with respect to the image, as each feature vector covers a large and potentially heterogeneous area of the image, *e.g.* both the object and the background. When visualizing (a part of) the network with features maps of higher-resolution, *i.e.*, with smaller receptive field, each point within the feature map corresponds to a smaller area of the original that is more likely to be homogeneous. To increase the attention map resolution, bi-linear or bi-cubic interpolations are commonly used for visualization. Nonetheless, these operations usually lead to blurry attention maps with no details [27, 25, 10, 30]. Another alternative is to consider larger input images as done in [12]. Nevertheless, this method inevitably increases the computation cost and also introduces relevant distortions

into original input images during the up-scaling procedure. Instead, we proposed to re-adapt the architecture of the CNN backbone used to prevent the reduction of the spatial resolution of feature maps. Concretely, this is achieved via reducing the stride of the last downsampling layers in the backbone network. By doing so, the resolution of the feature maps increased from 14×14 to 56×56 (cf. section 4.1). This limits the computation cost increase as only the feature maps of the last layers become larger.

To obtain a higher-resolution model without significant loss of performance, the distillation model proposed in [14] is employed. More specifically, a student network with increased resolution is trained to imitate the lower-resolution teacher network. When training the student network, the usual cross-entropy loss was employed jointly with the KL-divergence between the predictions of the student and teacher network to bridge the gap between the two models:

$$L = \frac{1}{N} \sum_i \alpha \text{CE}(\tilde{y}_s, y) + (1 - \alpha) \text{KL}(\tilde{y}_t || \tilde{y}_s), \quad (1)$$

where \tilde{y}_t, \tilde{y}_s denote the outputs of the teacher and student models, y is the ground truth and α is a parameter that balances the cross-entropy term and the KL divergence term.

3.2 Non-Parametric Attention Layer

In most cases, the object of interest is composed of several parts, where each part of the combination of parts potentially plays different roles in classification. Modern classification deep CNN models proceed original input and predict corresponding labels in an end-to-end manner, the extraction of important local parts, the modeling of their pairwise correlations, and their contribution to final classification are learned throughout the network. It is thus intuitively appealing to explore the pairwise correlations between the local object parts intermediate feature maps within the network and visualize the part-feature interactions as ‘attention’. In [20], features corresponding to each object part were aggregated separately to construct a feature matrix, i.e., a list of feature vectors. The separation of local object parts could be achieved via attention layers composed of multiple convolutional blocks [16], which is parametric.

With the burgeoning improvement of neural network architectures, state-of-the-art models achieve impressive performances on multiple large-scale benchmarks. Therefore, the backbone networks utilized in those models should be equipped with the capabilities in separating the local parts. Grounded by well-performing network architecture, instead of incorporating the usual attention neural module, a list of refined feature vectors are formed sequentially by grouping intermediate feature vectors with respect to their *activation* and their similarity with each other.

In this study, the *activation* level a of a feature vector f is quantified by its euclidean norm, i.e., $\|f\|^2$. The feature vector f , whose norm is one of the highest in the corresponding feature volume, is considered to be *active*. Furthermore, a feature vector is considered as singular if the other selected features are not similar to it.

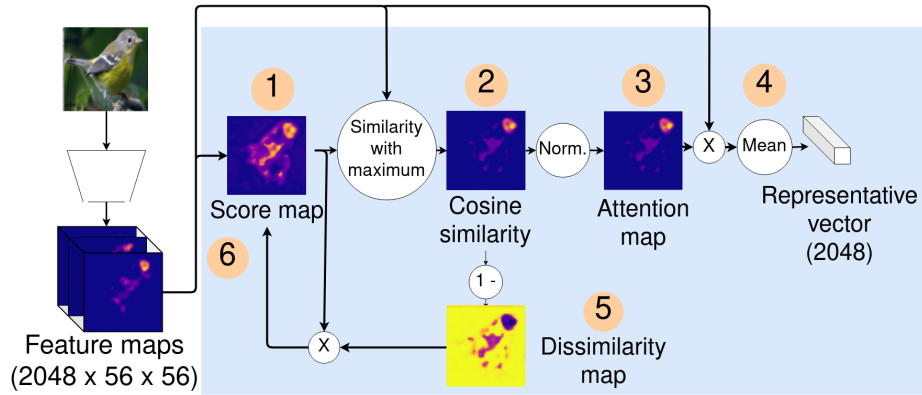


Figure 2: Illustration of the method used to group features without any dedicated module.

Algorithm 1 Identification of representative vectors $\{\hat{f}_k\}$

Input : feature vectors $\{f_i\}$

```
(1)  $a_i \leftarrow \|f_i\|^2$ 
for  $k = 1$  to  $N$  do
   $i_{max} \leftarrow \underset{i}{\operatorname{argmax}} a_i$ 
  for all  $i$  do
    (2)  $s_i \leftarrow \cos(f_i; f_{i_{max}})$ 
    (3)  $w_i \leftarrow s_i / \sum_{i'} s_{i'}$ 
    (4)  $\hat{f}_k \leftarrow \sum_i w_i \times f_i$ 
    (5,6)  $a_i \leftarrow (1 - w_i) \times a_i$ 
  end for
end for
return  $\hat{f}_1, \hat{f}_2, \dots, \hat{f}_N$ 
```

Alg. 1 and Fig. 2 summarize the proposed feature grouping algorithm. In a nutshell, it selects the top N active singular (i.e., not similar to each other) feature vectors from the feature volume and further refines them by aggregating them with similar vectors. This algorithm outputs an $N \times M$ feature matrix, where M is the dimension of the vectors. For simplicity, the feature vectors are indexed with only $i \in [0, H \cdot W - 1]$, where $H \times W$ is the resolution of the feature map. The i_{th} vector is denoted as f_i . The selection of N is discussed in the supplemental materials.

During the first interaction, each f_i was initialized with an activation score a_i equals to its euclidean norm (corresponds to Step 1 in Alg. 1 and Fig. 2). Afterwards, the vector with the highest norm is selected (Step 2). The motivation behind this procedure is that among all the feature vectors in the feature volume of a regular CNN, the ones with higher norms tend to have greater impacts on the final feature vector obtained after the pooling layer e.g., the average/max pooling. When employing a well-performing network architecture for a certain task, the high norm features are expected to be more discriminative than the ones with lower norm. Higher norm features are also supposed to contribute more to the final prediction. Hence, by selecting the high norm vector, we aim at reproducing this phenomenon in our architecture. This intuition is empirically verified in section 4.3, where experimental results show that accuracy decreases with random vectors selection or with only the 2_{nd} , 3_{rd} ranked features.

After obtaining the feature vector with the greatest norm value $f_{i_{max}}$, it is then refined with other features that are similar to it (Step 2 to 4). Concretely, the cosine similarity s_i between each feature f_i and $f_{i_{max}}$ is computed (Step 2). Subsequently, $\{s_i\}$ is normalized to yield weights $\{w_i\}$ such that $\sum_i w_i = 1$ (Step 3). The k_{th} feature vector \hat{f}_k is then obtained by computing the weighted average across all the vectors (Step 4). Afterward, a dissimilarity map $1 - w_i$ is computed by reversing the weights (Step 5) and the activation scores $\{a_i\}$ are updated by multiplying them by $1 - w_i$ for all i (Step 6). By doing so, it could be ensured that the new chosen location i_{max} and its estimation $f_{i_{max}}$ is different from the ones chosen in the previous iterations, while still extracting high norm vectors. The aforementioned procedure (line 3-8) is repeated for the $k + 1_{th}$ feature vectors until top- N feature vectors are computed. Lastly, the obtained $\hat{f}_1, \hat{f}_2, \dots, \hat{f}_N$ are concatenated and feed to the final classification layer. The weights $\{w_i\}$ corresponding to the top- N representative features serve as attention maps for highlighting local parts that contribute the most to the final decision-making of the task, with the rank of the features indicating the importance level of the respective object parts. It is worth noting that, as there are no extra attention neural layers integrated, our attention model is non-parametric. This scheme could be easily plugged into any modern deep neural network framework, where classification is associated.

4 Experiments

The proposed framework was evaluated on various computer vision tasks on relevant state-of-the-art benchmarks, including the fine-grained image classification [32, 23, 18], few-shot classification [5] and person re-identification [40]². For performance comparison regarding visualization, we compared the proposed BR-NPA attention model with the bilinear CNN (B-CNN) [21], which is considered as the baseline model and also state-of-the-art post-hoc algorithms dedicated to model visualization including Grad-CAM [27], Grad-CAM++ [6], Guided backpropagation [29] and also the baseline activation map (AM) method. These methodologies were selected as most CNN attention maps in the literature were generated using one of them.

The models which performance is reported from the literature in the fine-grained experiments were not applied to person re-identification or few-shot classification as they are complex methods specifically tailored for fine-grained classification. Only the variant of B-CNN proposed by [16] was re-implemented and showed poor performance on re-identification and few-shot classification. Also, the visualisations produced by these models come either from AM (MG-CNN) or a neural attention module (B-CNN, FCAN, MA-CNN, ProtoPNet). ST-CNN and 2-level attention produce no saliency map as the first directly predicts the crop to apply and the latter uses an object detector on random image patches to filter out the ones showing background. Therefore, visualisations from AM and neural attention module are provided, along with visualisations obtained from generic methods like Grad-CAM, Grad-CAM++, and Guided Grad-CAM++, to obtain a comprehensive and concise representation of the methods in the literature.

4.1 Implementation Details

To adapt B-CNN [21] for visualization, the features extracted from the backbone network were fed into a ResNet basic block [13] followed by a 1×1 convolution and a ReLU activation which output is used as the attention maps. The basic Resnet block is composed of 2 sequential convolutional layers (with the batch normalization and ReLU activation), and the residual connection followed by a final ReLU activation. Once obtained the attention maps, each map is multiplied with the feature volume before applying the pooling layer. In total C' feature vectors could be obtained (same number as attention maps). Finally, the vectors were concatenated and passed to a softmax layer. For all experiments across all tasks, hyper-parameters were estimated with a Tree-structured Parzen Estimator (TPE) from the Optuna framework [2], except in section 4.3, where we used the default hyper-parameter values. Details of how the proposed attention was adjusted and employed for different tasks are given below, where a similar recipe was applied for B-CNN. The 3 attention maps obtained with BR-NPA or B-CNN were visualized with an RGB mapping. The red, green, and blue channels of each pixel are used to represent its contribution w.r.t. the 1_{st} , 2_{nd} and 3_{rd} attention maps. The three channels are also multiplied by the norm of the corresponding feature vector, to make salient pixels brighter.

Fine-grained image classification: For both BR-NPA and the baseline model B-CNN, the ResNet-50 [13] pre-trained on the ImageNet dataset [26] was considered as the backbone network since it is one of the most commonly used network architectures in various domains.³ To obtain higher-resolution feature maps, the stride of the downsampling blocks in the 3_{rd} and 4_{th} layer of the ResNet-50 backbone network was set to 1 instead of 2, which increased the feature maps from 14×14 to 56×56 .

Few-shot classification: The MTL model proposed in [31] is one of the state-of-the-art meta/few-shot classification models. It was thus employed as a backbone with the proposed attention model for more comprehensive visualization. The average pooling layer in the backbone in MTL was replaced with the proposed attention layer, where 3 representative vectors were produced. The original classification layer was also extended to take the concatenation of the 3 representative features as input. To achieve more precise visualisation with higher-resolution, network distillation was conducted as detailed in section 3.1. The model was then trained as described in [31] on one of the standard few-shot classification benchmark dataset CIFAR-FS dataset [5]. In line with MTL, the ResNet-12 was used. The stride of the downsampling blocks in 2_{nd} and 3_{rd} layer of the ResNet-12 were set to 1 instead of 2. As a result, the resolution of the feature maps was enlarged from 10×10 to 40×40 .

²More results including more visualisations and more implementation details are available in supplementary material.

³Other adapted network architectures were also tested. More details and results are given in the supplemental materials.

Person re-identification: Similar to the setup for the few-shot classification task, one of the best-performing models proposed in [41], *i.e.*, the DG-Net, was adapted with our BR-NPA. Analogously, the average pooling layer in the identification module used by [41] was removed and replaced with our layer. Then, the model was trained as elucidated in [41] on the popular Market-1501 dataset [40]. It has to be emphasised that the DG-Net has a complex architecture that is difficult to train from scratch. Thus, we utilized the pretrained weights provided by the authors and modified the DG-Net architecture to speed up the training procedure. However, the proposed method extracts N feature vectors, whereas the original model extracts only one feature vector for classification. To prevent a size mismatch between the weights for the original dense layer with the feature vector extraction (512×2048) and the expanded dense layer ($512 \times 2048 \cdot N$), we duplicated the weights N times along the feature axis. This procedure was used to train DG-Net in combination with both BR-NPA and B-CNN. The ResNet-50 was used as backbone for the task of person re-identification to be consistent with [41]. The strides of the 2_{nd} and 3_{rd} layers of the ResNet-50 were set to 1 instead of 2, knowing that the stride of the 4_{th} layer was already set to 1 by the original authors. This increased the resolution of the feature maps from 16×8 to 64×32 .

4.2 Experimental Results

Fine-grained image classification: The performances of the proposed model and state-of-the-art visualization models in terms of accuracy on three fine-grained datasets, including the CUB-200-2011 [32], FGVC-Aircraft [23] and the Stanford cars [18] datasets are depicted in Table 1. It is shown that BR-NPA achieves state-of-the-art performances, and outperforms most of the other interpretability-oriented methods on the three datasets.

	Dataset		
Method	CUB	FGVC	Stanford cars
2-level attn. [34]	77.9	-	-
MG-CNN [33]	81.7	-	-
FCAN [22]	82.0	-	-
ST-CNN [17]	84.1	-	-
ProtoPNet [7]	84.8	-	-
B-CNN [21]	84.1	84.2	91.3
MA-CNN [39]	85.4	88.4	91.7
B-CNN (our impl.)	84.6	88.9	89.7
BR-NPA	85.5	89.6	91.7

Table 1: Performance for task of fine-grained classification.

Selected visualization of the attention maps are presented in Fig. 3 (a). Among all the images, the attention maps produced by BR-NPA highlight more precise details of the objects that capture well the inter-class unique characteristic. For example, in rows 4-6, highlighted finer-grained local regions are most of the time the tails or wings of the airplanes, which help to differ different airplane models. Similarly, B-CNN is also able to identify similar local important parts, but they are generally less precise. Conversely, the highlighted regions from Grad-CAM++ and AM approaches are significantly coarser, which cover the entire objects, while the ones from Guided Grad-CAM++ and Grad-CAM are sparse and spread out randomly all over the images. None of those attention regions provide precise information that helps the decision-making of fine-grained classification.

Person Id-reidentification: The accuracy of DG-Net equipped with different attention methods on one of the most common benchmark Market-1501 dataset [40] are illustrated in Table 9. Compared to other attention schemes, the lower-resolution version of BR-NPA achieves the best performances. Its performance is slightly poorer compared to the original DG-Net. Yet, as aforementioned, the complex architecture makes it hard to train from scratch, and we hence employed the pre-trained weights. One of the possible reason for the slight performance drop could be that the pre-trained network was not well adapted to our attention framework, and therefore are more prone to local optimum.

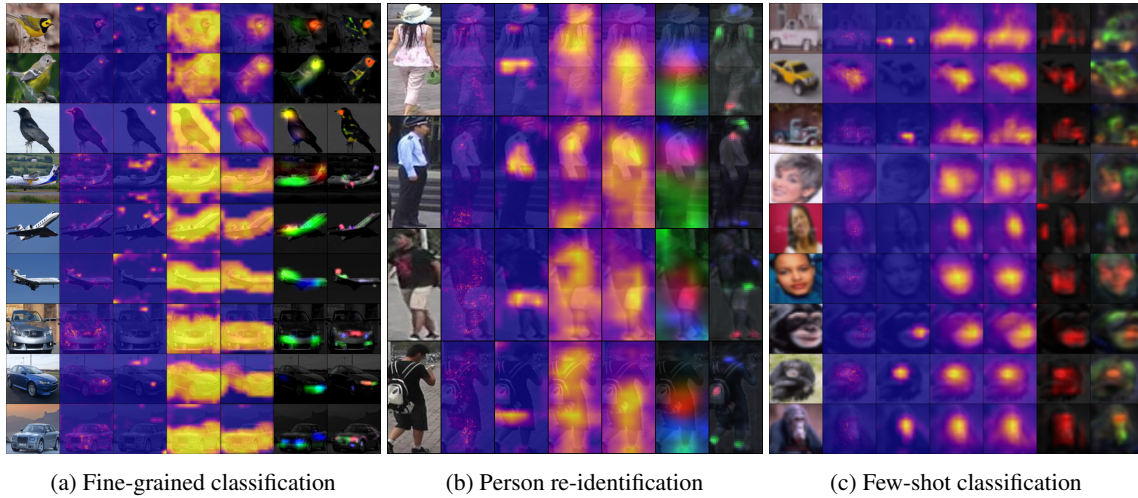


Figure 3: From left to right : original image, Guided Grad-CAM++, Grad-CAM, Grad-CAM++, AM, B-CNN, BR-NPA. The first four columns indicate saliency with a yellow color, whereas the last two rows indicate saliency using brightness and use colors to indicate by which map the pixel was attended. Red, green and blue represent the 1_{st} , 2_{nd} and 3_{rd} maps respectively.

Comprehensive attention maps are shown in Fig. 3 (b). Similar to fine-grained classification, the attention maps produced by BR-NPA emphasize local important details of the clothes on the person that are momentous for the ID re-identification regarding the significant intra-class variations across different cameras. For example, highlighted regions include shoes (rows 1-4), a logo on the bag (row 3), pockets (row 3), or epaulette (row 2), which help to differentiate different persons. B-CNN is only able to focus on larger parts of the person, e.g., the upper-body (rows 1-3) or the whole handbag (row 3). In contrast, the highlighted regions indicated by the AM Grad-CAM++ methods are significantly coarser, which are overlapped with the regions of the entire body, whereas the ones predicted by Grad-CAM and Guided Grad-CAM++ are again randomly distributed across the entire image without providing specific interpretable local information. The particular noisy aspect of Guided Grad-CAM++ on this task could be due to the high level of blur in the input compared to the images utilized in fine-grained classification. Moreover, the Guided-backpropagation-like methodologies have been proven to focus on edges[1], which are less robust to blurry, lower-resolution input. Let alone the negligible

Method	Attention	Resolution	Accuracy
DG-Net [41]	\times	16×8	94.8
	B-CNN	16×8	78.4
	BR-NPA	16×8	93.6
	BR-NPA	64×32	88.2

Table 2: Performance for task of person re-identification.

performance drops compared to the original DG-Net, it is showcased that our BR-NPA could be easily plugged in a complex pre-trained architecture without suffering from a significant loss of accuracy while providing insightful visualization.

Few-shot classification: The MTL model equipped with B-CNN and BR-NPA module was evaluated in a 1-shot 5-way few shot setting on the CIFAR-FS dataset [5]. Mean accuracy is summarized in Table 3. As observed, by integrating the higher-resolution version of BR-NPA, the accuracy of the original MTL model is improved, which is also superior to the version with B-CNN.

Representative visualized maps are depicted in in Fig. 3 (c). On one hand, as opposed to fine-grained classification and person re-identification, in the task of few-shot classification, attention maps generated by BR-

NPA highlight slighter larger areas of the object, while most of the local parts are still well determined and are distinguishable from each other. For instance, BR-NPA separates the wheels from the car body (rows 1-3) or the face from the hair (rows 4-6), which are all key relevant components for recognizing the corresponding categories. These observations demonstrate the feasibility of adapting BR-NPA for few-shot learning classifications. Interestingly, unlike the visualization maps obtained in the task of fine-grained classification, the model tends to focus on the entire objects instead of finer regions in a few-shot regime, which also verifies the interpretability of the proposed models across tasks. On the other hand, B-CNN is not able to differentiate different local parts as it fails to generate more than one attention map. The regions highlighted by the Grad-CAM++ and AM approaches also cover the entire object, while the ones obtained through Grad-CAM are sparse and highlight no particular area (rows 3-6). Furthermore, Again, Guided Grad-CAM++ produces very noisy maps due to blurry input, which weaken the magnitudes of edge-pixels [1].

Method	Attention	Resolution	Accuracy
MTL [31]	\times	10×10	61.7 ± 0.9
	B-CNN	10×10	58.1 ± 1.1
	BR-NPA	10×10	69.9 ± 0.9
	BR-NPA	40×40	65.7 ± 0.7

Table 3: Performance for task of few-shot classification.

Comparisons of attention maps obtained from different tasks: Obviously, the attention maps obtained from different tasks highlight the target object at different granularity-level. For the task of fine-grained classification and person re-identification, our method yields more precise attention maps that focus on finer object parts. Differently, for few-shot classification, the proposed model tends to focus on the entire object as the objective of few-shot is to distinguish between categories instead of sub-categories with only a few samples per unseen class. It is demonstrated that our model is able to generate interpretable visualized maps according to the goal of the task, which could provide important insights for the development of different methodologies, *i.e.*, different network architectures that pay more attention to a certain type of local areas, regarding the goal of the target task.

4.3 Ablation study ⁴

Impact of active feature selection and refinement strategy: Three ablative studies were conducted to explore the impacts of the proposed strategies of active feature vectors selection and the feature refinement on the performances, including (1) the ablative model where the feature vectors are uniformly and randomly selected among all available vectors instead of utilizing the active selection strategy; (2) the ablative model without the refinement phase, which simply concatenates all the active vectors and passes them directly to the classification layer; (3) a model with random selection and no refinement phase. During this ablation experiment, the aforementioned 3 ablative models along with the original model were trained with reduced strides to increase resolution (cf. section 4.1) without distillation or hyper-parameter optimisation for the sake of efficiency. Results concluded in Table 7 verifies the validity of both the active feature selection and refinement strategies.

The relevance of the representative vectors extracted via the proposed model: For this purpose, 5 classification layers were added to the network and were fed with a different set of representative vectors as input. Precisely, instead of receiving the 3 representative vectors, *i.e.*, $\{\hat{f}_1, \hat{f}_2, \hat{f}_3\}$, the 5 layers only receive the following vector or combination of vectors: $\{\hat{f}_1, \hat{f}_2\}$, $\{\hat{f}_2, \hat{f}_3\}$, $\{\hat{f}_1\}, \{\hat{f}_2\}$ and $\{\hat{f}_3\}$. Each additional layer was trained by adding a cross-entropy term to the loss function. By doing so, the final new loss function is an accumulation of the 6 cross-entropy terms. To prevent the supplementary layers from adjusting the feature vectors for their needs, we prevent their gradients from back-propagating to the features.

Similar to the previous ablation studies, the model with additional layers was trained in high-resolution without distillation. The accuracy of each of the supplementary layers (and the main layer) is summarized in Table 5. As shown, when using only one vector, performance decreases along with the ranking of the feature

⁴Due to limited space, only results for ablation study of fine-grained classification are presented, others are in the supplemental materials.

Raw vector selection method	Refining	Accuracy
Random	No	0.21
Random	Yes	0.53
Active	No	0.73
Active	Yes	0.81

Table 4: Results of ablation study.

vectors (from 1 to 3). Similarly, when removing one of the vectors from the full set, the accuracy also drops. This observation proves indirectly that the contribution of each attention map to the task is relevant to the ranking of the feature.

Vector(s)	$\{\hat{f}_1, \hat{f}_2, \hat{f}_3\}$	$\{\hat{f}_1, \hat{f}_2\}$	$\{\hat{f}_2, \hat{f}_3\}$	$\{\hat{f}_1\}$	$\{\hat{f}_2\}$	$\{\hat{f}_3\}$
Acc.	79.5	79.1	77.9	77.3	73.2	56.8

Table 5: Impact of number & rank of features on accuracy.

Increasing the resolution of feature map: The effects of using larger feature maps resolution on both the performances of B-CNN [20] and a BR-NPA were explored. They were both trained on the CUB-200-2011 dataset. We compared two resolutions including 14×14 and 56×56 . The first is the default output resolution and the second one was obtained by reducing the strides of layers 3 and 4 to 1. To train higher-resolution models, we employed distillation, as detailed in section 3.1.

Ideally, the attention map is expected to be sparse, *i.e.*, focusing on a small local area of the image. To quantify this, we introduce a new metric, namely, the *sparsity*. First, we averaged the multiple attention maps produced by the model. Then, to take the feature vector norm into account, each element of the map was multiplied by the corresponding feature vector euclidean norm. Finally, the sparsity is defined as $s = a_{max}/a_{mean}$, where a_{max} is the maximum of the resulting map and a_{mean} is its mean value. An attention map focusing on a small part of the image is supposed to have a low mean value which ends out with a high sparsity value. Conversely, a map covering all the input uniformly is supposed to have a maximum value that is close to its mean value. Therefore its sparsity is close to the minimum value, *i.e.*, 1. We are therefore looking for models with a high sparsity value. Distilling the higher-resolution model obtained via reducing strides helps to improve the sparsity of the student network with respect to the teacher network ($11.2 \rightarrow 19.6$ for B-CNN, and $7.46 \rightarrow 21.3$ for BR-NPA). This shows that distillation combined with reduction of striding helps to generate more precise, interpretable attentions map and improve the accuracy of the model. Results depicted in Table 6 shows that the higher-resolution models outperform their corresponding teacher network (+1.7 and +0.3 respectively for B-CNN and BR-NPA). For comparison, a CNN with default resolution (14×14) obtains an accuracy of 84.2%.

Model	Map size	Distillation	Accuracy	Sparsity
B-CNN	14×14	-	82.9	11.2
	56×56	✓	84.6	19.6
BR-NPA	14×14	-	85.2	7.46
	56×56	✓	85.5	21.3

Table 6: Impact of resolution on performance.

Additionally, we also evaluated the impact of increasing the resolution of the feature maps on the interpretability of the attention map qualitatively. We trained a student CNN to imitate a lower-resolution teacher CNN with distillation and visualize the activation maps for both the teacher and student CNN in Fig. 4. It could be observed that the attention maps from the higher-resolution CNN are more interpretable as they sparser and the activated areas are located on the sub-parts of the object instead of the whole object.



Figure 4: From left to right: original image, attention maps of CNN with lower and then higher-resolution feature maps.

4.4 Part discriminability hierarchy

Fig 5 shows visually whether there is a hierarchy *i.e.*, ranking of importance level among the parts' relevance that contributes to the decision-making of the task. For example, on the bird dataset, the first map (in red) focuses more on the head and the second map (green) focuses more on the body, indicating that the head is more discriminative than the body for the identification of the bird species.

Furthermore, the blue map is not visible on the bird dataset because it has focused on vectors with very low norms compared to ones selected by the red or green map. Low euclidean norm feature vectors have an ignorable impact on the final prediction of the task. In other words, these low-norm features are not relevant for the decision. The visualisation on the aircraft dataset shows that the three maps are often visible and each can focus on various parts like tails, wheels, engines, *etc.* This indicates that, according to the model, it is necessary to focus on three parts as they are of equivalent importance level. Similarly, on the cars dataset, the first and second maps focus on the front air inlet and the lights, whereas the blue maps tend to target more other details like the flasher (column 2) or the car body details (column 1). It is shown that the two most important parts are the front air inlet and the lights and that some details like the body details are also but less discriminative. It is showcased that BR-NPA facilitates the discovery of the importance-level hierarchy among the object's parts according to their relevance.

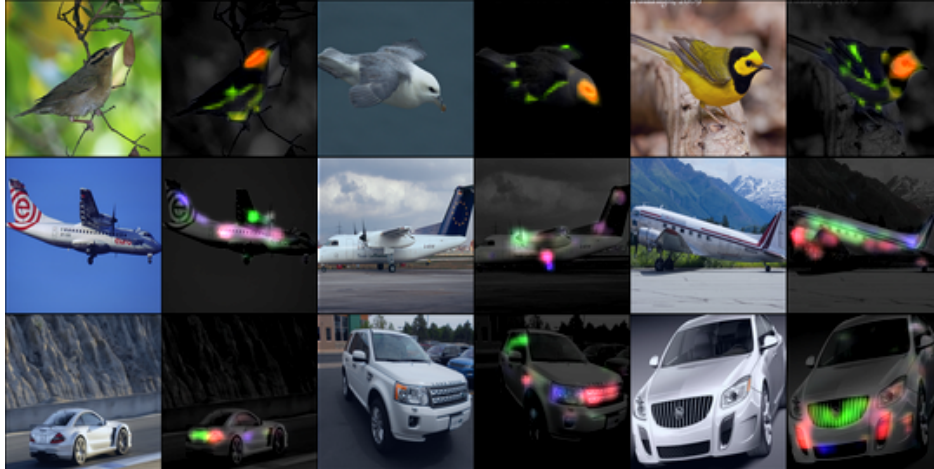


Figure 5: Attention maps produced by BR-NPA.

4.5 Memory footprint and efficiency

Last but not least, BR-NPA has a smaller memory footprint and requires less inference time compared to B-CNN for various backbones, while obtaining better accuracy. Relevant results and analysis are in the supplemental materials.

5 Conclusion

In this work, we proposed a non-parametric attention that can be easily integrated into an existing architecture to significantly improve its interpretability while maintaining its accuracy. Specifically, this method improves the usual neural attention mechanism in two ways. First, the feature maps resolution was increased using distillation to highlight finer details. Second, the neural layer was replaced by a well-designed non-parametric module such that the importance level of the parts composing the object can be visualised using color. Furthermore, it is an easy plugin that could be applied to various problems like fine-grained classification, re-identification, and few-shot classification and produces saliency maps matching the task objective. Contrarily to the usual attention, it is easy to integrate it in a complex pretrained architecture without significant accuracy loss. In the future, we will run a subjective study to investigate the use of BR-NPA in understanding computer-assisted decisions.

References

- [1] Julius Adebayo, Justin Gilmer, Michael Muelly, Ian Goodfellow, Moritz Hardt, and Been Kim. Sanity checks for saliency maps. In S. Bengio, H. Wallach, H. Larochelle, K. Grauman, N. Cesa-Bianchi, and R. Garnett, editors, *Advances in Neural Information Processing Systems*, volume 31. Curran Associates, Inc., 2018. 8, 9
- [2] Takuya Akiba, Shotaro Sano, Toshihiko Yanase, Takeru Ohta, and Masanori Koyama. Optuna: A next-generation hyperparameter optimization framework, 2019. 6
- [3] Dzmitry Bahdanau, Kyunghyun Cho, and Yoshua Bengio. Neural machine translation by jointly learning to align and translate. *arXiv preprint arXiv:1409.0473*, 2014. 1, 2
- [4] Jasmijn Bastings and Katja Filippova. The elephant in the interpretability room: Why use attention as explanation when we have saliency methods? *arXiv preprint arXiv:2010.05607*, 2020. 1, 2
- [5] Luca Bertinetto, Joao F. Henriques, Philip Torr, and Andrea Vedaldi. Meta-learning with differentiable closed-form solvers. In *International Conference on Learning Representations*, 2019. 6, 8
- [6] A. Chattopadhyay, A. Sarkar, P. Howlader, and V. N. Balasubramanian. Grad-cam++: Generalized gradient-based visual explanations for deep convolutional networks. In *2018 IEEE Winter Conference on Applications of Computer Vision (WACV)*, pages 839–847, 2018. 3, 6
- [7] Chaofan Chen, Oscar Li, Alina Barnett, Jonathan Su, and Cynthia Rudin. This looks like that: deep learning for interpretable image recognition. In *NeurIPS*, 2019. 3, 7
- [8] G. Chen, J. Lu, M. Yang, and J. Zhou. Learning recurrent 3d attention for video-based person re-identification. *IEEE Transactions on Image Processing*, 29:6963–6976, 2020. 3
- [9] Marius Cordts, Mohamed Omran, Sebastian Ramos, Timo Rehfeld, Markus Enzweiler, Rodrigo Benenson, Uwe Franke, Stefan Roth, and Bernt Schiele. The cityscapes dataset for semantic urban scene understanding. In *Proc. of the IEEE Conference on Computer Vision and Pattern Recognition (CVPR)*, 2016. 18
- [10] Abhimanyu Dubey, Otkrist Gupta, Pei Guo, Ramesh Raskar, Ryan Farrell, and Nikhil Naik. Pairwise confusion for fine-grained visual classification, 2018. 3
- [11] Tianyu Gao, Xu Han, Zhiyuan Liu, and Maosong Sun. Hybrid attention-based prototypical networks for noisy few-shot relation classification. *Proceedings of the AAAI Conference on Artificial Intelligence*, 33(01):6407–6414, Jul. 2019. 3
- [12] W. Ge, X. Lin, and Y. Yu. Weakly supervised complementary parts models for fine-grained image classification from the bottom up. In *2019 IEEE/CVF Conference on Computer Vision and Pattern Recognition (CVPR)*, pages 3029–3038, 2019. 3
- [13] K. He, X. Zhang, S. Ren, and J. Sun. Deep residual learning for image recognition. In *2016 IEEE Conference on Computer Vision and Pattern Recognition (CVPR)*, pages 770–778, 2016. 3, 6
- [14] Geoffrey Hinton, Oriol Vinyals, and Jeff Dean. Distilling the knowledge in a neural network, 2015. 4

- [15] Ruibing Hou, Hong Chang, Bingpeng MA, Shiguang Shan, and Xilin Chen. Cross attention network for few-shot classification. In H. Wallach, H. Larochelle, A. Beygelzimer, F. d'Alché-Buc, E. Fox, and R. Garnett, editors, Advances in Neural Information Processing Systems, volume 32. Curran Associates, Inc., 2019. 3
- [16] Tao Hu and Honggang Qi. See better before looking closer: Weakly supervised data augmentation network for fine-grained visual classification. CoRR, abs/1901.09891, 2019. 3, 4, 6
- [17] Max Jaderberg, Karen Simonyan, Andrew Zisserman, and koray kavukcuoglu. Spatial transformer networks. In C. Cortes, N. D. Lawrence, D. D. Lee, M. Sugiyama, and R. Garnett, editors, Advances in Neural Information Processing Systems 28, pages 2017–2025. Curran Associates, Inc., 2015. 3, 7
- [18] Jonathan Krause, Michael Stark, Jia Deng, and Li Fei-Fei. 3d object representations for fine-grained categorization. In 4th International IEEE Workshop on 3D Representation and Recognition (3dRR-13), Sydney, Australia, 2013. 6, 7
- [19] Wei Li, Xiatian Zhu, and Shaogang Gong. Harmonious attention network for person re-identification. In Proceedings of the IEEE Conference on Computer Vision and Pattern Recognition (CVPR), June 2018. 3, 21
- [20] T. Lin, A. RoyChowdhury, and S. Maji. Bilinear cnn models for fine-grained visual recognition. In 2015 IEEE International Conference on Computer Vision (ICCV), pages 1449–1457, 2015. 3, 4, 10
- [21] Tsung-Yu Lin, Aruni RoyChowdhury, and Subhransu Maji. Bilinear cnn models for fine-grained visual recognition. In Proceedings of the 2015 IEEE International Conference on Computer Vision (ICCV), ICCV '15, pages 1449–1457, Washington, DC, USA, 2015. IEEE Computer Society. 6, 7
- [22] Xiao Liu, Tian Xia, Jiang Wang, Yi Yang, Feng Zhou, and Yuanqing Lin. Fully convolutional attention networks for fine-grained recognition. arXiv: Computer Vision and Pattern Recognition, 2016. 3, 7
- [23] S. Maji, J. Kannala, E. Rahtu, M. Blaschko, and A. Vedaldi. Fine-grained visual classification of aircraft. Technical report, 2013. 6, 7
- [24] Akash Kumar Mohankumar, Preksha Nema, Sharan Narasimhan, Mitesh M Khapra, Balaji Vasan Srinivasan, and Balaraman Ravindran. Towards transparent and explainable attention models. arXiv preprint arXiv:2004.14243, 2020. 1
- [25] Yuxin Peng, Xiangteng He, and Junjie Zhao. Object-part attention model for fine-grained image classification. IEEE Transactions on Image Processing, 27(3):1487–1500, Mar 2018. 3
- [26] Olga Russakovsky, Jia Deng, Hao Su, Jonathan Krause, Sanjeev Satheesh, Sean Ma, Zhiheng Huang, Andrej Karpathy, Aditya Khosla, Michael Bernstein, Alexander C. Berg, and Li Fei-Fei. ImageNet Large Scale Visual Recognition Challenge. International Journal of Computer Vision (IJCV), 115(3):211–252, 2015. 6
- [27] R. R. Selvaraju, M. Cogswell, A. Das, R. Vedantam, D. Parikh, and D. Batra. Grad-cam: Visual explanations from deep networks via gradient-based localization. In 2017 IEEE International Conference on Computer Vision (ICCV), pages 618–626, 2017. 1, 2, 3, 6
- [28] Jianlou Si, Honggang Zhang, Chun-Guang Li, Jason Kuen, Xiangfei Kong, Alex C. Kot, and Gang Wang. Dual attention matching network for context-aware feature sequence based person re-identification. In Proceedings of the IEEE Conference on Computer Vision and Pattern Recognition (CVPR), June 2018. 3, 21
- [29] Jost Tobias Springenberg, Alexey Dosovitskiy, Thomas Brox, and Martin A. Riedmiller. Striving for simplicity: The all convolutional net. CoRR, abs/1412.6806, 2015. 3, 6
- [30] Guolei Sun, Hisham Cholakkal, Salman Khan, Fahad Shahbaz Khan, and Ling Shao. Fine-grained recognition: Accounting for subtle differences between similar classes, 2019. 3
- [31] Qianru Sun, Yaoyao Liu, Tat-Seng Chua, and Bernt Schiele. Meta-transfer learning for few-shot learning. In The IEEE Conference on Computer Vision and Pattern Recognition (CVPR), June 2019. 6, 9
- [32] C. Wah, S. Branson, P. Welinder, P. Perona, and S. Belongie. The Caltech-UCSD Birds-200-2011 Dataset. Technical Report CNS-TR-2011-001, California Institute of Technology, 2011. 6, 7
- [33] D. Wang, Z. Shen, J. Shao, W. Zhang, X. Xue, and Z. Zhang. Multiple granularity descriptors for fine-grained categorization. In 2015 IEEE International Conference on Computer Vision (ICCV), pages 2399–2406, 2015. 3, 7
- [34] Tianjun Xiao, Yichong Xu, Kuiyuan Yang, Jiaxing Zhang, Yuxin Peng, and Zheng Zhang. The application of two-level attention models in deep convolutional neural network for fine-grained image classification. 2015. 7
- [35] Shipeng Yan, Songyang Zhang, and Xuming He. A dual attention network with semantic embedding for few-shot learning. Proceedings of the AAAI Conference on Artificial Intelligence, 33(01):9079–9086, Jul. 2019. 3
- [36] Yuhui Yuan, Xilin Chen, and Jingdong Wang. Object-contextual representations for semantic segmentation. arXiv preprint arXiv:1909.11065, 2020. 18, 19
- [37] Hongguang Zhang, Li Zhang, Xiaojuan Qi, Hongdong Li, Philip H. S. Torr, and Piotr Koniusz. Few-shot action recognition with permutation-invariant attention. In Andrea Vedaldi, Horst Bischof, Thomas Brox, and Jan-Michael Frahm, editors, Computer Vision – ECCV 2020, pages 525–542, Cham, 2020. Springer International Publishing. 3

- [38] Zhizheng Zhang, Cuiling Lan, Wenjun Zeng, Xin Jin, and Zhibo Chen. Relation-aware global attention for person re-identification. In Proceedings of the IEEE/CVF Conference on Computer Vision and Pattern Recognition (CVPR), June 2020. 3, 19, 21
- [39] H. Zheng, J. Fu, T. Mei, and J. Luo. Learning multi-attention convolutional neural network for fine-grained image recognition. In 2017 IEEE International Conference on Computer Vision (ICCV), pages 5219–5227, 2017. 3, 7
- [40] L. Zheng, L. Shen, L. Tian, S. Wang, J. Wang, and Q. Tian. Scalable person re-identification: A benchmark. In 2015 IEEE International Conference on Computer Vision (ICCV), pages 1116–1124, 2015. 6, 7
- [41] Zhedong Zheng, Xiaodong Yang, Zhiding Yu, Liang Zheng, Yi Yang, and Jan Kautz. Joint discriminative and generative learning for person re-identification. In IEEE Conference on Computer Vision and Pattern Recognition (CVPR), 2019. 7, 8, 19, 21
- [42] Bolei Zhou, Aditya Khosla, Àgata Lapedriza, Aude Oliva, and Antonio Torralba. Learning deep features for discriminative localization. CoRR, abs/1512.04150, 2015. 2
- [43] Yaohui Zhu, Chenlong Liu, and Shuqiang Jiang. Multi-attention meta learning for few-shot fine-grained image recognition. In Christian Bessiere, editor, Proceedings of the Twenty-Ninth International Joint Conference on Artificial Intelligence, IJCAI-20, pages 1090–1096. International Joint Conferences on Artificial Intelligence Organization, 7 2020. Main track. 3

A Introduction

This supplementary material provides more contents including: (1) an extended characterization of BR-NPA with an extended ablation study. This study further shows the impact of the proposed feature selection and refinement strategies on visualizations for tasks of person re-identification and fine-grained classification; (2) results that showcase the advantages of the proposed BR-NPA in terms of efficiency and memory footprint; (3) extensive experimental results of BR-NPA on semantic segmentation, which demonstrate again the feasibility of plugging the proposed framework into complex pretrained network architecture; (4) more experimental results compared to state-of-the-art attention model designed for person re-identification; (5) extra visualization results for the considered tasks mentioned in the paper along with novel visualized results for task of semantic segmentation.

B BR-NPA characterization

B.1 Visualization of the Ablative Models

In this section more visual friendly results of the ablation studies regarding the proposed active feature selection and refinement strategy are provided. Table 7 recalls the performance of the 3 variants: (1) the ablative model, where the feature vectors are uniformly and randomly selected among all available vectors; (2) the ablative model without the refinement phase; (3) the ablative model with random selection and no refinement phase. Attention maps obtained with the 3 ablative models are depicted in Fig. 6. As shown, selecting random vectors, instead of the high norm ones, ends out into highlighting parts that are not contributing to decision makings (i.e., parts that are not imperative for classification). Moreover, without feature refinement, it is difficult to interpret which of the model is contributing.

Raw vector selection method	Refining	Accuracy
Random	No	0.21
Random	Yes	0.53
Active	No	0.73
Active	Yes	0.81

Table 7: Results of ablation study.

B.2 Impact of the number of attention map accuracy

To improve the visualization and interpretability of the attention maps, we chose $N = 3$. However, the selection of N may have an influence on performances. To verify this, we further examined different N values and checked the corresponding accuracy of both B-CNN and BR-NPA for the task of fine-grained classification. Results are shown in Fig. 7. It is observed that by varying N the performances do not change significantly for both models. Furthermore, also that BR-NPA consistently yields better accuracy than B-CNN.

B.3 Training Stability

To evaluate the impact of the non-parametric attention layer on gradient properties, we propose to visualise the gradient euclidean norm of the 3 last convolutional layers of the ResNet-50 backbone before the attention layer. Fig. 8 shows that, during training, the non-parametric layer produces gradient with much smaller norm variance, yielding smoother training.



Figure 6: From left to right : the original image, a BR-NPA selecting random vectors without refinement, a BR-NPA selecting random vectors, a BR-NPA without refinement and a BR-NPA selecting high norm vectors and refining them. Selecting random vectors leads to focus on irrelevant parts of the input and not refining them makes it difficult to understand on which part the model has focused.

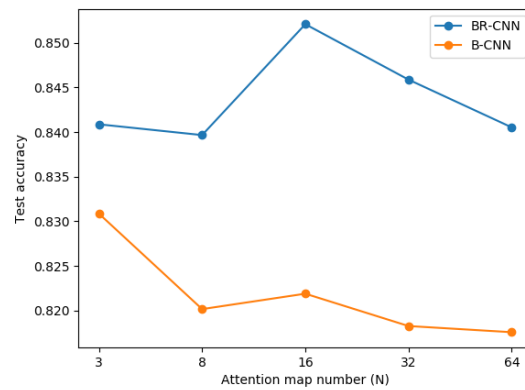


Figure 7: Impact of the attention map number N on the test accuracy.

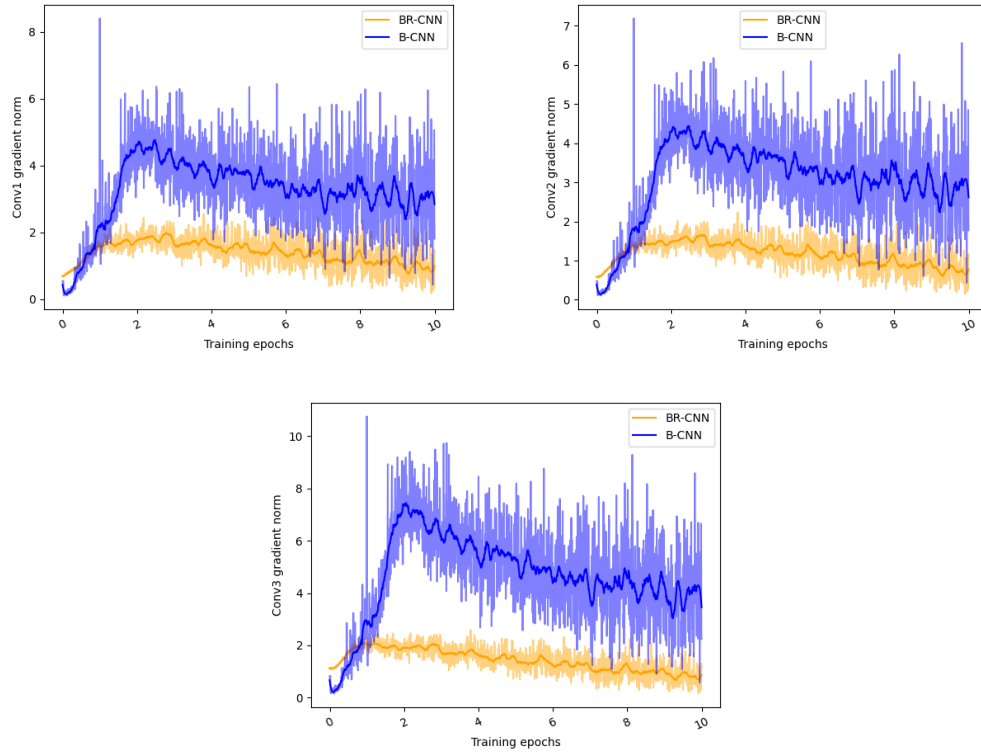


Figure 8: Gradient norm of the three last convolution layers with the non-parametric attention layer (BR-NPA) and with the usual neural layer (B-CNN). BR-NPA yields gradient with much smaller norm variance, yielding smoother training.

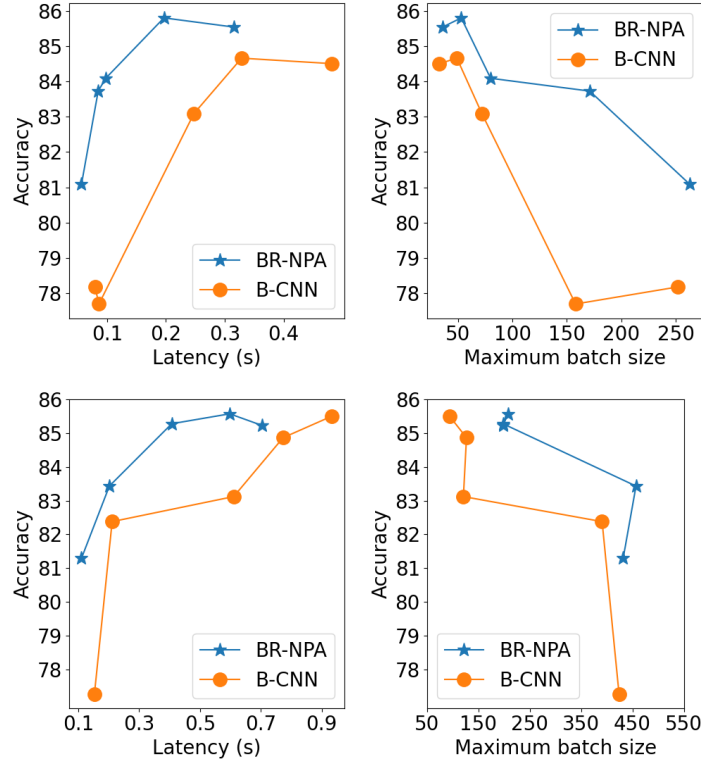


Figure 9: Comparison of B-CNN and BR-NPA efficiency during training. Left: training latency for higher and lower-resolution. Right: maximum batch size for higher and lower-resolution. Measures are done on two GPUs with a total memory of 32GB. Latency includes both the forward and the backward pass. Our attention layer is consistently more efficient than B-CNN both in terms of latency and memory footprint.

B.4 Efficiency of BR-NPA

We also compared the training execution time and memory footprint of BR-NPA with B-CNN. Both of them were set to produce 14×14 feature maps. First, we computed the times required to process a batch of 10 images at resolution 448×448 during training for several backbones including the ResNet-18, ResNet-34, ResNet-50, ResNet-101 and the ResNet-152. Fig. 9 reports the execution time in seconds observed over 100 batches. The results demonstrate that BR-NPA is faster than B-CNN on average. When training for a certain backbone network, we also computed the size of the biggest batch that can fit on 2 GPU. Each with a memory of 16G. Fig. 9 shows that BR-NPA consumes less GPU memory than B-CNN. One of the main reasons why BR-NPA has better memory footprint and efficiency is that the outer product computed by B-CNN between the attention and the features maps results in a larger tensor with size of $(N \times C \times C' \times H \times W)$ ⁵. In addition, BR-NPA computes the attention maps and the corresponding feature vectors one after another, instead of all at once, without producing such a large tensor.

C Semantic segmentation

Implementation details: The proposed method was also incorporated in one of the state-of-the-art semantic segmentation models, *i.e.*, the OCR-net [36], and was evaluated on the Cityscapes dataset [9]. In [36], object

⁵ N, C, C', H and W are the batch size, the feature number, the attention maps number and the height and width of the features respectively.

Method	Attention	Resolution	Mean IoU
OCR [36]	\times	256×512	81.1
	BR-NPA	256×512	80.8

Table 8: Performance of OCR with our method compared with the default attention layer on the Cityscapes dataset.

region representations vectors were computed by multiplying each initial probability map by the feature volume, followed by a global average pooling. This was replaced with the following procedure. First, the feature vector with the highest initial probability was selected for each class. By such, L vectors could be obtained, where L is the number of classes in the dataset. Akin to the aforementioned tasks, these vectors were then refined with similar vectors. Afterwards, each vector f was replaced by the weighted mean of all vectors, where the weights are the normalized similarities regarding f . After generating L refined vectors, they were then used for representing object regions. Apart from aforementioned procedure, the model was trained as in [36]. Similarly to DG-Net, OCR-net is an architecture that is difficult to train from scratch therefore we used pretrained weights provided by the authors to speed training up. By combining OCR-net and BR-NPA, no layer had its size modified which is why, contrarily to DG-Net, the pre-existing weights did not have to be adapted. We did not use distillation to obtain higher resolution attention maps on this task as the feature maps resolution is by default (256×512) which is already sufficient for visualisation.

During the refinement phase, to make full use of the OCR architecture and reduce the amount of noise in the final representative vectors, the cosine similarities were multiplied by the probability map of the corresponding class produced by the auxiliary layer. This allows to use the knowledge embedded in the pretrained weights to focus on the relevant vectors of the feature maps.

Results: Attention maps of the semantic segmentation task are shown in Fig. 10 and the mean IoUs are reported in Table 8. As mentioned before, the OCR-Net is also an architecture that is difficult to train from scratch. Hence, we used pretrained weights to speed the training up. Again, the pretrained weights may not be adapted to our architecture and the model is prone to convergence at local optima, which explains the slight accuracy loss observed by integrating BR-NPA. However, this demonstrate again that our method can be plug in a pretrained architecture without suffering from significant accuracy loss and provide comprehensive visualization.

D More Visualisation Results

Supplementary visualization of the attention maps are presented in Figs. 11, 12 and 13.

D.1 Stability Across View Points

Fig. 14 shows that BR-NPA is able to identify key parts of the target object and is robust to the change of view point.

D.2 Comparison with RGA [38]

We also compared BR-NPA with the RGA module [38]. For fair comparison, the RGA modules were integrated in the DG-Net backbone and trained as elucidated in [41]. Concretely, [38] proposes to add one spatial attention and one channel attention module after each ResNet-50 layer (which is also the backbone used by DG-Net). Therefore, the ResNet-50 weights pretrained on person re-identification can be loaded and the attention layers are randomly initialised. The fourth spatial attention layer is followed by the average pooling layer. Therefore, similarly to the procedure conducted for BR-NPA and B-CNN visualisations, each pixel on the map is multiplied by the norm of the corresponding feature vector.

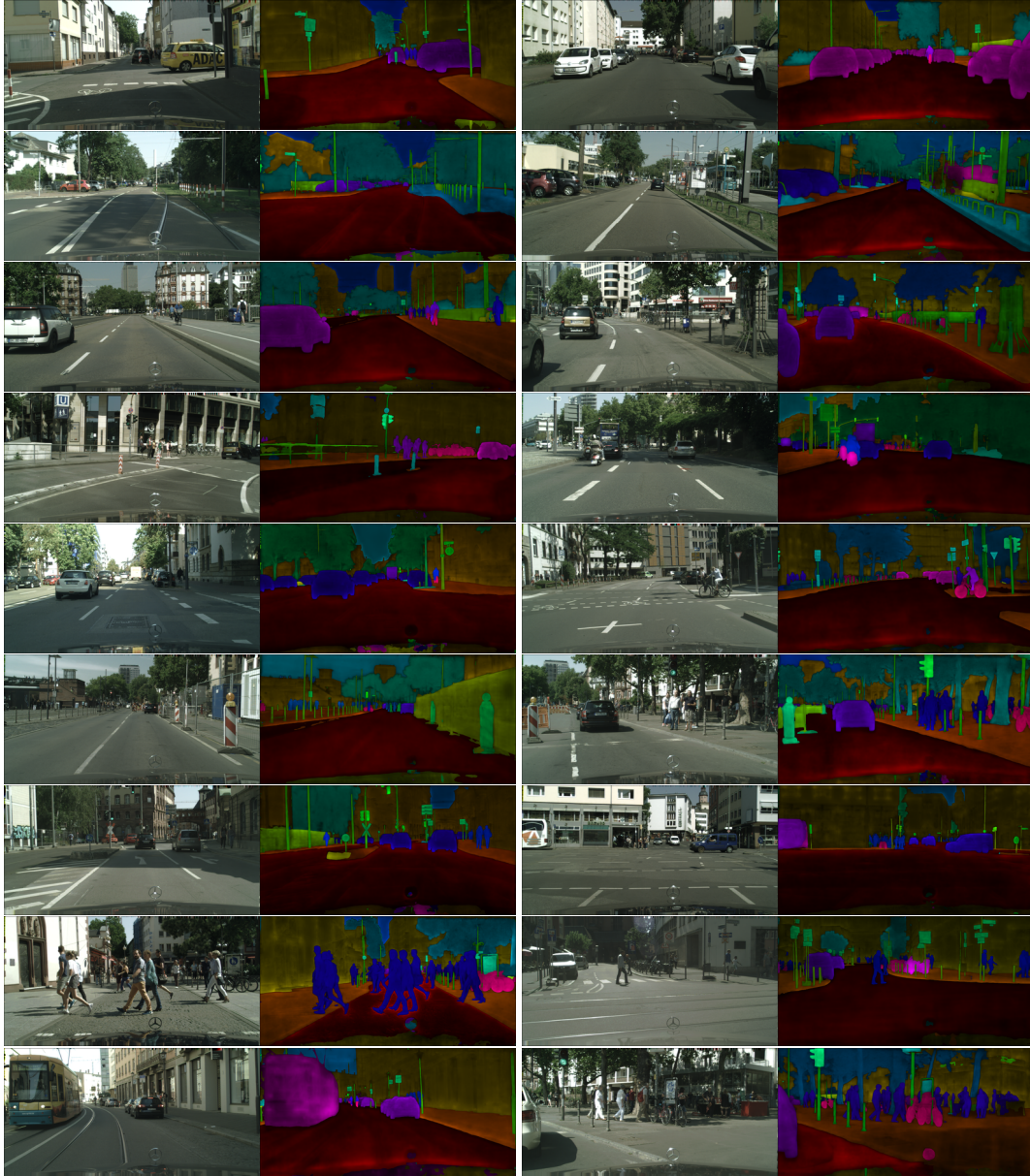


Figure 10: Attention maps obtained with our method applied to the OCR net on the Cityscapes dataset. Color indicates the predicted class and pixel intensity indicates the contribution to the corresponding object region representation vector. The darker the color, the more contributions to the decision making. One can see that, contrarily to fine-grained classification, the attention maps focus less on details but more on the whole segment/region uniformly.

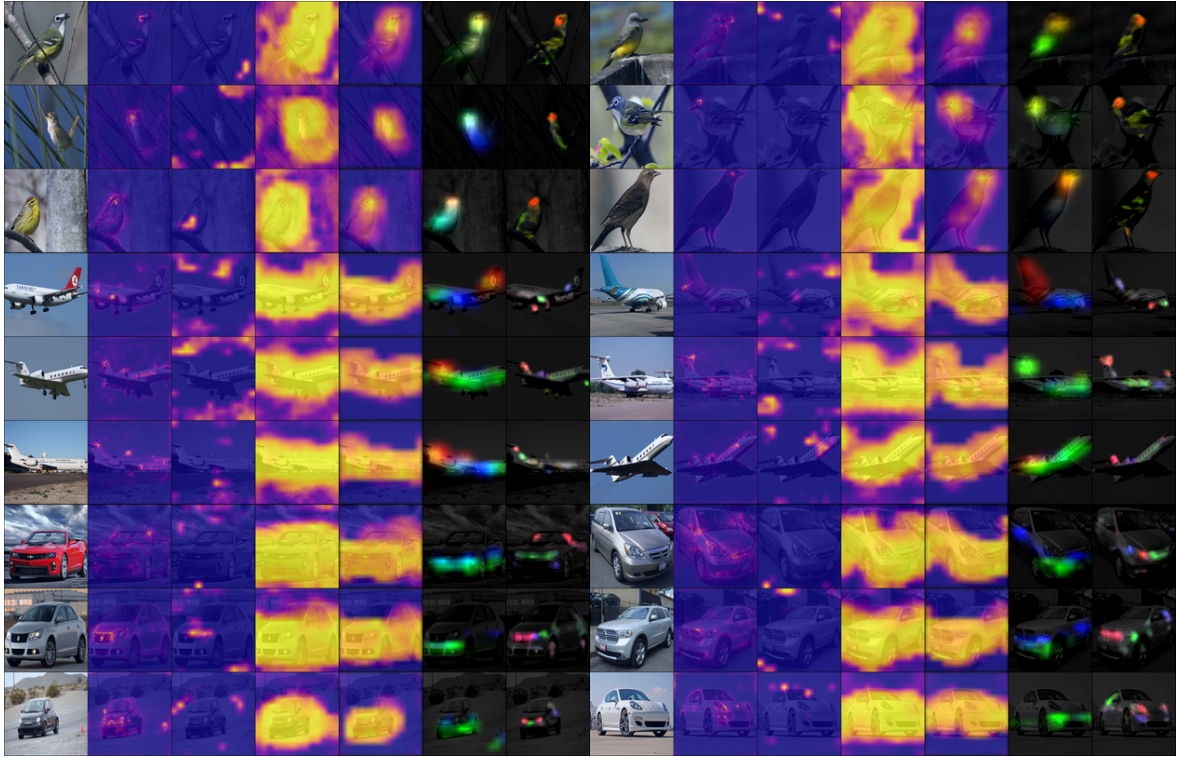


Figure 11: Visual comparison on the fine-grained tasks.

Table 9 summarizes the results. It can be seen that RGA achieves similar accuracy to BR-NPA. Nevertheless, as shown in Fig. 15, it is worth emphasizing that the attention maps generated by RGA are significantly less interpretable, where the first and second maps do not even seem to focus on the object of interest.

Method	Attention	Resolution(s)	Accuracy
DG-Net [41]	X	16×8	94.8
	B-CNN	16×8	78.4
	BR-NPA	16×8	93.6
	BR-NPA	64×32	88.2
	RGA [38]	16×8	93.0
		32×16	
		64×32	
		128×64	
Harm. att. [19]	Harmonious	160×64 40×16 10×4	91.2
Dual att. [28]	Dual	8×4	91.42

Table 9: Performance for task of person re-identification.

References

- [1] Julius Adebayo, Justin Gilmer, Michael Muelly, Ian Goodfellow, Moritz Hardt, and Been Kim. Sanity checks for saliency maps. In S. Bengio, H. Wallach, H. Larochelle, K. Grauman, N. Cesa-Bianchi, and R. Garnett, editors, *Advances in Neural Information Processing Systems*, volume 31. Curran Associates, Inc., 2018. 8, 9

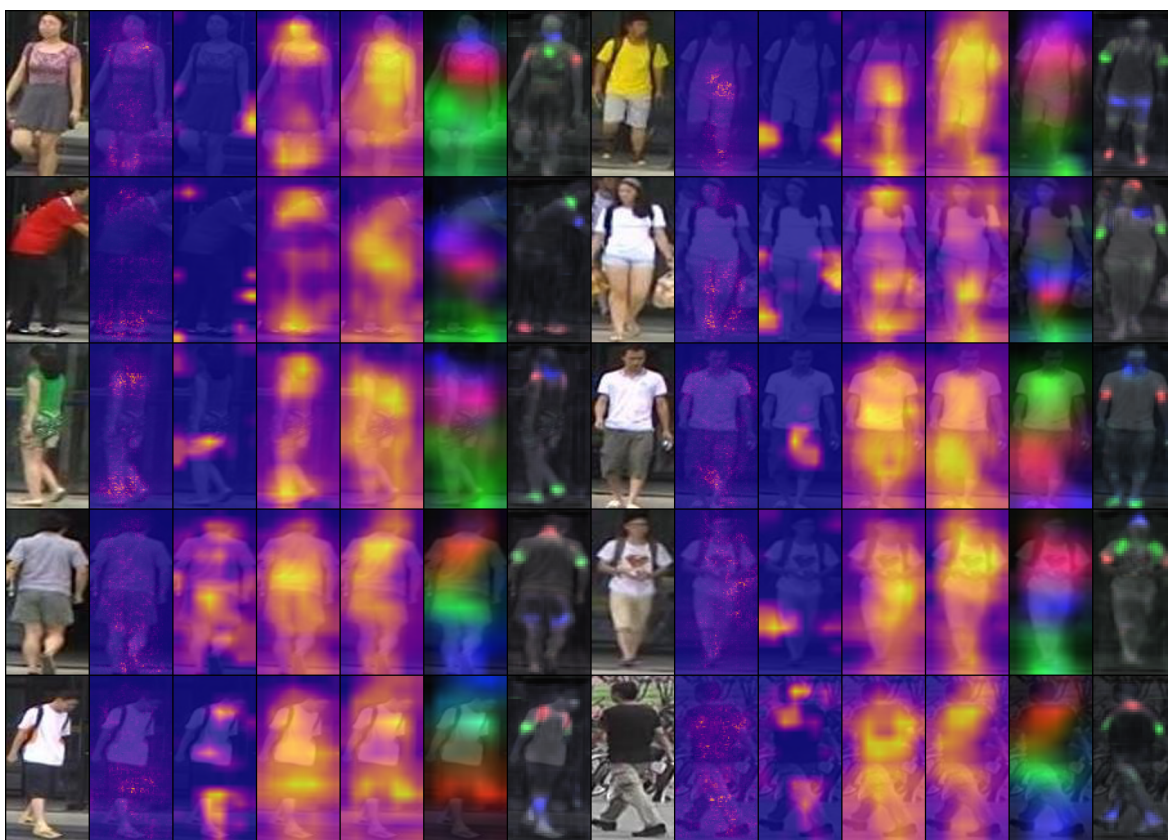


Figure 12: Visual comparison on the person re-identification task.

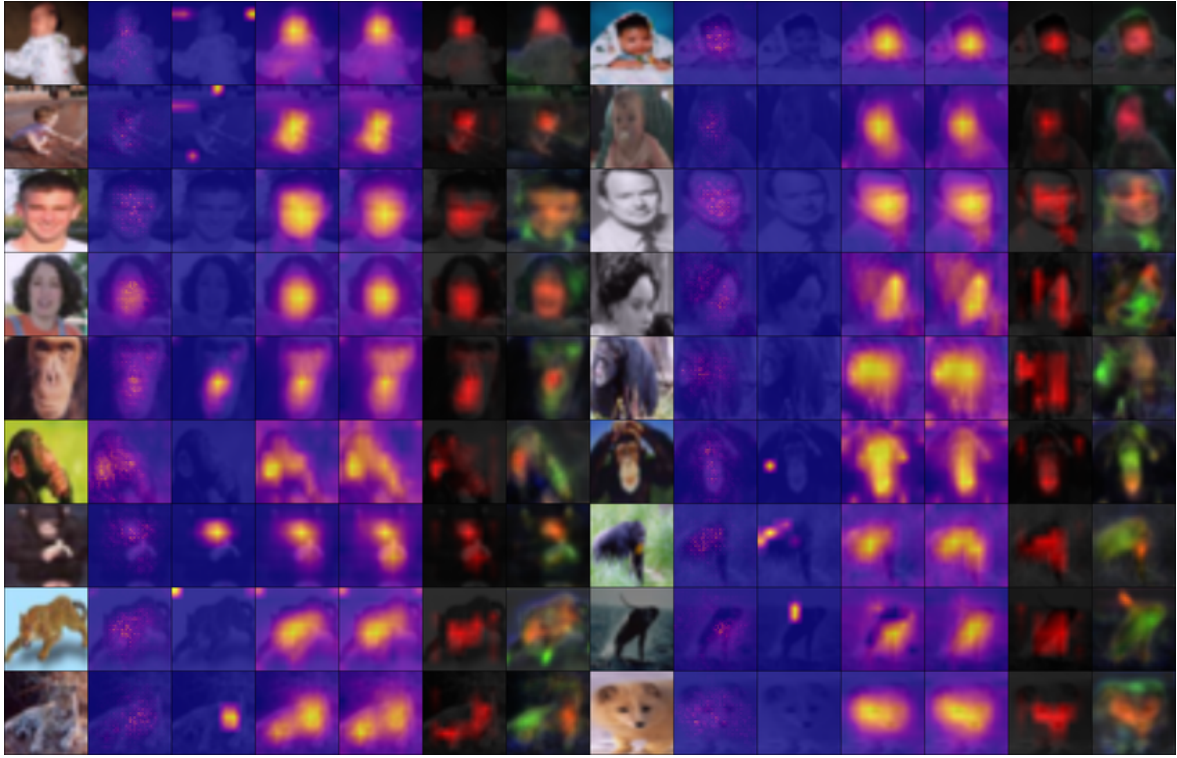


Figure 13: Visual comparison on the few-shot classification task.



Figure 14: The parts focused on by BR-NPA are robust across view points.

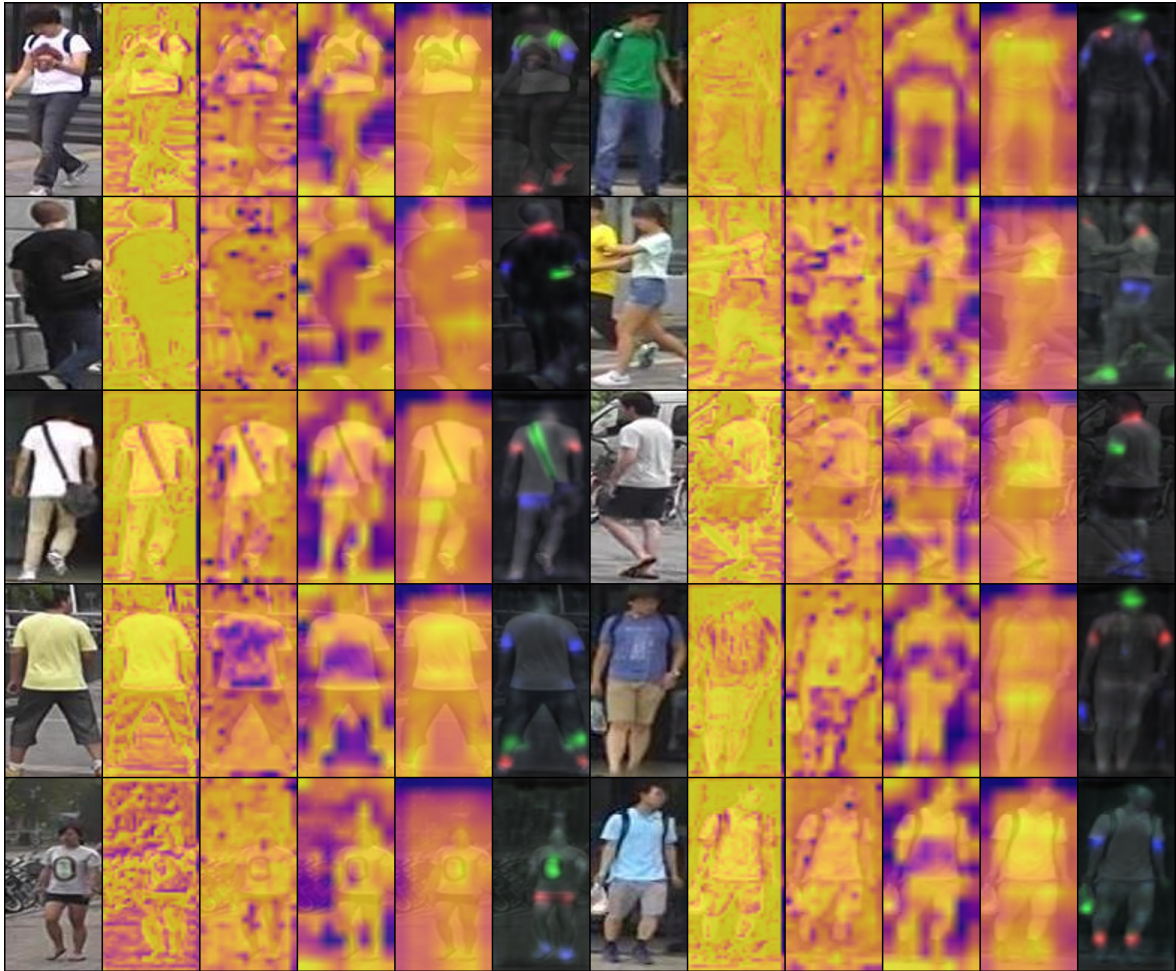


Figure 15: From left to right: original image, the four spatial attention maps produced by RGA and the attentions maps produced by BR-NPA.

- [2] Takuya Akiba, Shotaro Sano, Toshihiko Yanase, Takeru Ohta, and Masanori Koyama. Optuna: A next-generation hyperparameter optimization framework, 2019. [6](#)
- [3] Dzmitry Bahdanau, Kyunghyun Cho, and Yoshua Bengio. Neural machine translation by jointly learning to align and translate. *arXiv preprint arXiv:1409.0473*, 2014. [1](#), [2](#)
- [4] Jasmijn Bastings and Katja Filippova. The elephant in the interpretability room: Why use attention as explanation when we have saliency methods? *arXiv preprint arXiv:2010.05607*, 2020. [1](#), [2](#)
- [5] Luca Bertinetto, Joao F. Henriques, Philip Torr, and Andrea Vedaldi. Meta-learning with differentiable closed-form solvers. In *International Conference on Learning Representations*, 2019. [6](#), [8](#)
- [6] A. Chattopadhyay, A. Sarkar, P. Howlader, and V. N. Balasubramanian. Grad-cam++: Generalized gradient-based visual explanations for deep convolutional networks. In *2018 IEEE Winter Conference on Applications of Computer Vision (WACV)*, pages 839–847, 2018. [3](#), [6](#)
- [7] Chaofan Chen, Oscar Li, Alina Barnett, Jonathan Su, and Cynthia Rudin. This looks like that: deep learning for interpretable image recognition. In *NeurIPS*, 2019. [3](#), [7](#)
- [8] G. Chen, J. Lu, M. Yang, and J. Zhou. Learning recurrent 3d attention for video-based person re-identification. *IEEE Transactions on Image Processing*, 29:6963–6976, 2020. [3](#)
- [9] Marius Cordts, Mohamed Omran, Sebastian Ramos, Timo Rehfeld, Markus Enzweiler, Rodrigo Benenson, Uwe Franke, Stefan Roth, and Bernt Schiele. The cityscapes dataset for semantic urban scene understanding. In *Proc. of the IEEE Conference on Computer Vision and Pattern Recognition (CVPR)*, 2016. [18](#)
- [10] Abhimanyu Dubey, Otkrist Gupta, Pei Guo, Ramesh Raskar, Ryan Farrell, and Nikhil Naik. Pairwise confusion for fine-grained visual classification, 2018. [3](#)
- [11] Tianyu Gao, Xu Han, Zhiyuan Liu, and Maosong Sun. Hybrid attention-based prototypical networks for noisy few-shot relation classification. *Proceedings of the AAAI Conference on Artificial Intelligence*, 33(01):6407–6414, Jul. 2019. [3](#)
- [12] W. Ge, X. Lin, and Y. Yu. Weakly supervised complementary parts models for fine-grained image classification from the bottom up. In *2019 IEEE/CVF Conference on Computer Vision and Pattern Recognition (CVPR)*, pages 3029–3038, 2019. [3](#)
- [13] K. He, X. Zhang, S. Ren, and J. Sun. Deep residual learning for image recognition. In *2016 IEEE Conference on Computer Vision and Pattern Recognition (CVPR)*, pages 770–778, 2016. [3](#), [6](#)
- [14] Geoffrey Hinton, Oriol Vinyals, and Jeff Dean. Distilling the knowledge in a neural network, 2015. [4](#)
- [15] Ruibing Hou, Hong Chang, Bingpeng MA, Shiguang Shan, and Xilin Chen. Cross attention network for few-shot classification. In H. Wallach, H. Larochelle, A. Beygelzimer, F. d’Alché-Buc, E. Fox, and R. Garnett, editors, *Advances in Neural Information Processing Systems*, volume 32. Curran Associates, Inc., 2019. [3](#)
- [16] Tao Hu and Honggang Qi. See better before looking closer: Weakly supervised data augmentation network for fine-grained visual classification. *CoRR*, abs/1901.09891, 2019. [3](#), [4](#), [6](#)
- [17] Max Jaderberg, Karen Simonyan, Andrew Zisserman, and koray kavukcuoglu. Spatial transformer networks. In C. Cortes, N. D. Lawrence, D. D. Lee, M. Sugiyama, and R. Garnett, editors, *Advances in Neural Information Processing Systems 28*, pages 2017–2025. Curran Associates, Inc., 2015. [3](#), [7](#)
- [18] Jonathan Krause, Michael Stark, Jia Deng, and Li Fei-Fei. 3d object representations for fine-grained categorization. In *4th International IEEE Workshop on 3D Representation and Recognition (3dRR-13)*, Sydney, Australia, 2013. [6](#), [7](#)
- [19] Wei Li, Xiatian Zhu, and Shaogang Gong. Harmonious attention network for person re-identification. In *Proceedings of the IEEE Conference on Computer Vision and Pattern Recognition (CVPR)*, June 2018. [3](#), [21](#)
- [20] T. Lin, A. RoyChowdhury, and S. Maji. Bilinear cnn models for fine-grained visual recognition. In *2015 IEEE International Conference on Computer Vision (ICCV)*, pages 1449–1457, 2015. [3](#), [4](#), [10](#)
- [21] Tsung-Yu Lin, Aruni RoyChowdhury, and Subhransu Maji. Bilinear cnn models for fine-grained visual recognition. In *Proceedings of the 2015 IEEE International Conference on Computer Vision (ICCV)*, ICCV ’15, pages 1449–1457, Washington, DC, USA, 2015. IEEE Computer Society. [6](#), [7](#)
- [22] Xiao Liu, Tian Xia, Jiang Wang, Yi Yang, Feng Zhou, and Yuanqing Lin. Fully convolutional attention networks for fine-grained recognition. *arXiv: Computer Vision and Pattern Recognition*, 2016. [3](#), [7](#)
- [23] S. Maji, J. Kannala, E. Rahtu, M. Blaschko, and A. Vedaldi. Fine-grained visual classification of aircraft. Technical report, 2013. [6](#), [7](#)
- [24] Akash Kumar Mohankumar, Preksha Nema, Sharan Narasimhan, Mitesh M Khapra, Balaji Vasan Srinivasan, and Balaraman Ravindran. Towards transparent and explainable attention models. *arXiv preprint arXiv:2004.14243*, 2020. [1](#)
- [25] Yuxin Peng, Xiangteng He, and Junjie Zhao. Object-part attention model for fine-grained image classification. *IEEE Transactions on Image Processing*, 27(3):1487–1500, Mar 2018. [3](#)

- [26] Olga Russakovsky, Jia Deng, Hao Su, Jonathan Krause, Sanjeev Satheesh, Sean Ma, Zhiheng Huang, Andrej Karpathy, Aditya Khosla, Michael Bernstein, Alexander C. Berg, and Li Fei-Fei. ImageNet Large Scale Visual Recognition Challenge. *International Journal of Computer Vision (IJCV)*, 115(3):211–252, 2015. 6
- [27] R. R. Selvaraju, M. Cogswell, A. Das, R. Vedantam, D. Parikh, and D. Batra. Grad-cam: Visual explanations from deep networks via gradient-based localization. In *2017 IEEE International Conference on Computer Vision (ICCV)*, pages 618–626, 2017. 1, 2, 3, 6
- [28] Jianlou Si, Honggang Zhang, Chun-Guang Li, Jason Kuen, Xiangfei Kong, Alex C. Kot, and Gang Wang. Dual attention matching network for context-aware feature sequence based person re-identification. In *Proceedings of the IEEE Conference on Computer Vision and Pattern Recognition (CVPR)*, June 2018. 3, 21
- [29] Jost Tobias Springenberg, Alexey Dosovitskiy, Thomas Brox, and Martin A. Riedmiller. Striving for simplicity: The all convolutional net. *CoRR*, abs/1412.6806, 2015. 3, 6
- [30] Guolei Sun, Hisham Cholakkal, Salman Khan, Fahad Shahbaz Khan, and Ling Shao. Fine-grained recognition: Accounting for subtle differences between similar classes, 2019. 3
- [31] Qianru Sun, Yaoyao Liu, Tat-Seng Chua, and Bernt Schiele. Meta-transfer learning for few-shot learning. In *The IEEE Conference on Computer Vision and Pattern Recognition (CVPR)*, June 2019. 6, 9
- [32] C. Wah, S. Branson, P. Welinder, P. Perona, and S. Belongie. The Caltech-UCSD Birds-200-2011 Dataset. Technical Report CNS-TR-2011-001, California Institute of Technology, 2011. 6, 7
- [33] D. Wang, Z. Shen, J. Shao, W. Zhang, X. Xue, and Z. Zhang. Multiple granularity descriptors for fine-grained categorization. In *2015 IEEE International Conference on Computer Vision (ICCV)*, pages 2399–2406, 2015. 3, 7
- [34] Tianjun Xiao, Yichong Xu, Kuiyuan Yang, Jiaxing Zhang, Yuxin Peng, and Zheng Zhang. The application of two-level attention models in deep convolutional neural network for fine-grained image classification. 2015. 7
- [35] Shipeng Yan, Songyang Zhang, and Xuming He. A dual attention network with semantic embedding for few-shot learning. *Proceedings of the AAAI Conference on Artificial Intelligence*, 33(01):9079–9086, Jul. 2019. 3
- [36] Yuhui Yuan, Xilin Chen, and Jingdong Wang. Object-contextual representations for semantic segmentation. *arXiv preprint arXiv:1909.11065*, 2020. 18, 19
- [37] Hongguang Zhang, Li Zhang, Xiaojuan Qi, Hongdong Li, Philip H. S. Torr, and Piotr Koniusz. Few-shot action recognition with permutation-invariant attention. In Andrea Vedaldi, Horst Bischof, Thomas Brox, and Jan-Michael Frahm, editors, *Computer Vision – ECCV 2020*, pages 525–542, Cham, 2020. Springer International Publishing. 3
- [38] Zhizheng Zhang, Cuiling Lan, Wenjun Zeng, Xin Jin, and Zhibo Chen. Relation-aware global attention for person re-identification. In *Proceedings of the IEEE/CVF Conference on Computer Vision and Pattern Recognition (CVPR)*, June 2020. 3, 19, 21
- [39] H. Zheng, J. Fu, T. Mei, and J. Luo. Learning multi-attention convolutional neural network for fine-grained image recognition. In *2017 IEEE International Conference on Computer Vision (ICCV)*, pages 5219–5227, 2017. 3, 7
- [40] L. Zheng, L. Shen, L. Tian, S. Wang, J. Wang, and Q. Tian. Scalable person re-identification: A benchmark. In *2015 IEEE International Conference on Computer Vision (ICCV)*, pages 1116–1124, 2015. 6, 7
- [41] Zhedong Zheng, Xiaodong Yang, Zhiding Yu, Liang Zheng, Yi Yang, and Jan Kautz. Joint discriminative and generative learning for person re-identification. In *IEEE Conference on Computer Vision and Pattern Recognition (CVPR)*, 2019. 7, 8, 19, 21
- [42] Bolei Zhou, Aditya Khosla, Àgata Lapedriza, Aude Oliva, and Antonio Torralba. Learning deep features for discriminative localization. *CoRR*, abs/1512.04150, 2015. 2
- [43] Yaohui Zhu, Chenlong Liu, and Shuqiang Jiang. Multi-attention meta learning for few-shot fine-grained image recognition. In Christian Bessiere, editor, *Proceedings of the Twenty-Ninth International Joint Conference on Artificial Intelligence, IJCAI-20*, pages 1090–1096. International Joint Conferences on Artificial Intelligence Organization, 7 2020. Main track. 3